UNIVERSITY OF AMSTERDAM

UvA-DARE (Digital Academic Repository)

Photophysics of perylene monoimide-labelled organocatalysts

Zheng, D.; Oskouei, M.R.; Sanders, H.J.; Qian, J.; Williams, R.M.; Brouwer, A.M.

DOI
10.1039/c8pp00462e

Publication date
2019

Document Version
Final published version

Published in
Photochemical & Photobiological Sciences

License
Article 25fa Dutch Copyright Act (https://www.openaccess.nl/en/policies/open-access-in-dutch-copyright-law-taverne-amendment)

Link to publication

Citation for published version (APA):
Zheng, D., Oskouei, M. R., Sanders, H. J., Qian, J., Williams, R. M., & Brouwer, A. M. (2019). Photophysics of perylene monoimide-labelled organocatalysts. *Photochemical & Photobiological Sciences*, *18*(2), 524-533. https://doi.org/10.1039/c8pp00462e

General rights
It is not permitted to download or to forward/distribute the text or part of it without the consent of the author(s) and/or copyright holder(s), other than for strictly personal, individual use, unless the work is under an open content license (like Creative Commons).

Disclaimer/Complaints regulations
If you believe that digital publication of certain material infringes any of your rights or (privacy) interests, please let the Library know, stating your reasons. In case of a legitimate complaint, the Library will make the material inaccessible and/or remove it from the website. Please Ask the Library: https://uba.uva.nl/en/contact, or a letter to: Library of the University of Amsterdam, Secretariat, P.O. Box 19185, 1000 GD Amsterdam, The Netherlands. You will be contacted as soon as possible.

UvA-DARE is a service provided by the library of the University of Amsterdam (https://dare.uva.nl)

Download date:13 Sept 2026

Photochemical & Photobiological Sciences

PAPER

View Article Online
View Journal | View Issue

Published on 13 December 2018. Downloaded by Universiteit van Amsterdam on 4/7/2020 1:17:18 PM.

Check for updates

Cite this: *Photochem. Photobiol. Sci.*, 2019, **18**, 524

Photophysics of perylene monoimide-labelled organocatalysts†

Dongdong Zheng, Mina Raeisolsadati Oskouei, Hans J. Sanders, Junhong Qian, ‡ René M. Williams and Albert M. Brouwer *

Received 16th October 2018,
Accepted 13th December 2018

DOI: 10.1039/c8pp00462e

rsc.li/pps

We designed and synthesized cinchona alkaloid derivates **PMI-BnCPD**, **1** and **PMI-dHQD**, **2**, in which a fluorescent perylene monoimide unit is linked to the quinuclidine fragment. The latter acts as an electron donor, quenching the perylene imide fluorescence in polar solvents. In the organocatalytic application of these compounds, the electron donor is deactivated by binding to an electrophile, *e.g.* H^+. We show that this restores the fluorescence, allowing the compounds to signal the electrophile binding step that occurs in many catalytic reactions. In order to demonstrate that charge transfer is indeed the fluorescence quenching mechanism, we detected the charge separated state by means of transient absorption spectroscopy. Incidentally, the excited state absorption bands of the locally excited and charge transfer states are very similar. The activity of the fluorophore labeled organocatalyst **1** in a fluorogenic Michael addition reaction is demonstrated.

1 Introduction

Quinine and other cinchona alkaloids that can be extracted from the bark of the cinchona ledgeriana tree have played a pivotal medicinal role in human society for a long time.[1] Nowadays, cinchona alkaloids (quinine, quinidine, cinchonine, and cinchonidine) are also well established powerful chiral auxiliaries and catalysts, successfully employed in numerous asymmetric chemical transformations.[2–9]

Perylene monoimide (PMI) is a chromophore with strong absorption and efficient fluorescence in the visible spectral range, and it has a high photochemical stability.[10–13] PMI derivatives are widely applied in (supra)molecular dye chemistry as photo- and electro-active units connected to *e.g.* oligothiophene,[14,15] polyphenylene oligomers[16,17] or dendrimers,[18,19] triphenylamine derivatives,[20–23] zinc porphyrin[24–26] or C_{60}-derivatives.[27] Their brightness and photostability also makes perylene bisimides useful for applications in single molecule chemistry.[28–30]

In the past years, widespread usage of cinchona alkaloid derived organocatalysts has been reported, and a classical reaction model for hydrogen bonding in organocatalysis was proposed by Wynberg as early as in 1977.[31,32] Later, many mechanisms for this kind of reactions were investigated, most of them based on computational methodology.[6,33,34] It would be interesting to use the native fluorescence of the cinchona alkaloids[35–38] to gain insight into the mechanisms of cinchona organocatalysis, but the short wavelengths of absorption renders them unsuitable for the most powerful single molecule techniques, which require absorption and fluorescence in the visible to near IR range. In the present work we designed two new fluorescent probes: cinchona alkaloid catalysts (BnCPD and dHQD) functionalized with a perylene monoimide (PMI) fluorophore. This can be excited with visible light and has strong fluorescence, allowing for future single molecule experiments on organocatalysis. In such experiments, the fluorophore can be used simply as a marker, *e.g.* to signal transient binding to a glass slide to which a reactant has been attached.[39] In the PMI derivatives studied here, an additional possibility is the detection of the binding of electrophilic reagents to the quinuclidine nitrogen atom. This is a nucleophilic or basic catalytic site, and it can interact as an electron donor quenching the fluorescence of the PMI unit. Binding/unbinding of electrophilic agents thus leads to fluorescence modulation in polar solvents. More generally, molecular systems in which photoinduced intramolecular electron transfer efficiently quenches the excited state of the chromophore form an important class of chemosensory materials.[40–46]

In this paper we describe and analyze the photophysical processes of compounds **1** and **2** (Scheme 1), in solvents of different polarities, ranging from toluene to acetonitrile. The dynamics of excited state electron transfer of **1** and **2** are studied using fluorescence spectroscopy.

van 't Hoff Institute for Molecular Sciences, University of Amsterdam, P.O. Box 94157, 1090 GD Amsterdam, The Netherlands. E-mail: a.m.brouwer@uva.nl

† Electronic supplementary information (ESI) available: Syntheses, product analysis, instrumentation, data processing, additional spectral data. See DOI: 10.1039/c8pp00462e

‡ Present address: East China University of Science and Technology, 130 Meilong Road, 200237 Shanghai, China.

This journal is © The Royal Society of Chemistry and Owner Societies 2019

Published on 13 December 2018. Downloaded by Universiteit van Amsterdam on 4/7/2020 1:17:18 PM.

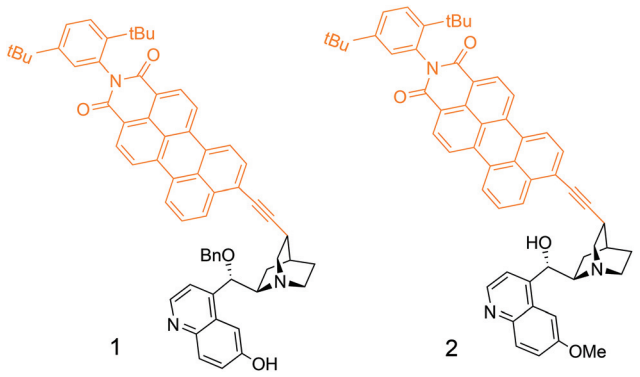

Scheme 1 Structure diagrams of the systems used in this study. PMI-BnCPD, **1** consists of a PMI (orange) and a 9-benzylcupreidine moiety (black). PMI-dHQD, **2** consists of PMI and dehydroquinidine (black).

Femtosecond transient absorption spectroscopy was used to further characterize the excited-state dynamics of PMI-BnCPD **1** in a series of solvents. The relaxation processes in the first ~10 ps are reflected by shifts in the transient absorption spectra. In polar solvents the absorption bands of charge-transfer states are detected. These are quite similar to those of the locally excited state, but still can be distinguished using a global spectrotemporal analysis. Organocatalytic activity of PMI-BnCPD **1** is demonstrated using benzylthiol and a fluorogenic BODIPY dye.

2 Experimental details

All experimental details are provided in the ESI.†

3 Results and discussion

3.1 Optical properties

3.1.1 UV-vis absorption and emission spectroscopy. Representative absorption and fluorescence spectra of **1** and **2** are shown in Fig. 1. Spectra in other solvents are in the ESI.† Numerical data are presented in Table 1. The absorption maxima are not very solvent dependent, but the red shift of the emission maximum with solvent polarity indicates solvent relaxation, as discussed below.

For both systems **1** and **2**, the fluorescence quantum yields and decay times show a strong solvent dependence. As can be seen from Table 1, with the increase of solvent polarity, the quantum yields (Φ_f) of **1** and **2** decrease. Those of **2** are relatively lower in the polar solvents. In non-polar solvents, all Φ_f values are larger and reach a maximum of 0.76 in toluene. A similar trend with solvent polarity can also be observed for the fluorescence lifetimes (τ_f) of the two compounds.

They decrease with increasing solvent polarity as seen in Table 1. The lifetimes of **2** are shorter than those of **1** in all polar solvents, and a small extent of quenching is already observed in THF. In the polar solvents, in addition to the dominant short-lived species, a long-lived component was detected, with a relative amplitude <3% (see ESI, Table S1†) and a decay time of ~4 ns. This small component is attributed to a PMI-containing impurity that lacks the electron donor group, and this was confirmed means of HPLC analysis (see Fig. S1, ESI†). The radiative rate constant is practically the same in all cases: $k_f = (1.8 \pm 0.2) \times 10^8\ s^{-1}$. Only in the case of **2** in polar solvents the calculated radiative rate is a bit higher, but this is probably due to the overestimation of Φ_f due to the contribution of the impurity. The quenching of the fluorescence of **1** and **2** in more polar solvents can be attributed to electron transfer from the quinuclidine electron donor to the PMI acceptor, as discussed below.

The addition of trifluoroacetic acid (TFA) has a very large effect on Φ_f and τ_f of the two compounds in polar solvents: under these acidic conditions, all of the values are restored to the high emission level as in non-polar solvents (see Table 1). Protonation of the amine by the strong acid suppresses the electron transfer process of **1** and **2** in polar solvents and restores the local PMI emission. This response could be reversed by the addition of base.

The driving force for excited state intramolecular electron transfer (charge separation, CS) can be estimated using eqn (1).[47]

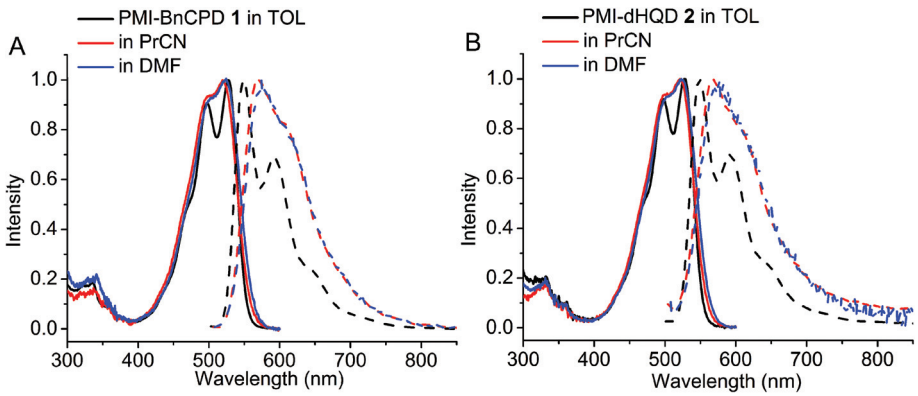

Fig. 1 Static absorption (solid lines) and emission spectra (dashed lines; λ_{exc} = 488 nm) of PMI-BnCPD **1** (A) and PMI-dHQD **2** (B) in various solvents.

Published on 13 December 2018. Downloaded by Universiteit van Amsterdam on 4/7/2020 1:17:18 PM.

Table 1 Absorption and fluorescence properties of PMI-BnCPD **1** and PMI-dHQD **2** in different solvents with and without trifluoroacetic acid (TFA)

	Solvent	Dielectric constant	UV/vis absorption	Fluorescence emission					
			$\lambda_{max,\ abs}$[a] (nm)	$\varepsilon \times 10^{-4}$[b] ($M^{-1}$ cm^{-1})	$\lambda_{max,\ em}$[c] (nm)	Φ_f[d]	τ_f[e] (ns)	Φ_f[d,f] (TFA)	τ_f[e,f] (ns) (TFA)
1	Tol	2.38	528	6.03	550	0.76	3.9	0.77	3.8
	DCM	9.1	522	6.27	563	0.75	4.3	0.77	4.2
	THF	7.5	523	5.56	559	0.73	4.0	0.73	4.1
	PrCN	20.7	521	6.92	570	0.21	1.3	0.72	4.1
	MeCN	37.5	520	5.70	578	0.07	0.38	0.71	4.4
	DMF	38	524	5.23	578	0.05	0.25	0.70	4.2
2	Tol	2.38	527	6.11	548	0.75	3.9	0.77	3.9
	DCM	9.1	522	6.23	561	0.75	4.2	0.78	4.2
	THF	7.5	522	5.64	557	0.67	3.9	0.73	4.1
	PrCN	20.7	520	6.51	567	0.10	0.48	0.72	4.2
	MeCN	37.5	518	5.67	566	0.05	0.15	0.69	4.4
	DMF	38	524	5.46	575	0.03	0.10	0.72	4.2

[a] Wavelength of maximum absorbance. [b] Molar absorption coefficient. [c] Wavelength of fluorescence maximum. [d] Fluorescence quantum yield. [e] Fluorescence decay time. [f] In the presence of TFA.

$$\Delta G_{CS} = e[E_{ox}\ (D/D^+) - E_{red}(A/A^-)] - E_{00} - \frac{e^2}{4\pi\varepsilon_0\varepsilon_S R_{CC}} - \frac{e^2}{8\pi\varepsilon_0}\left(\frac{1}{r^+}+\frac{1}{r^-}\right)\left(\frac{1}{\varepsilon_{ref}}-\frac{1}{\varepsilon_S}\right) \quad (1)$$

For compounds **1** and **2**, the standard electrode potentials (E_{red} (D^+/D) and E_{red} (A/A^-)) of the donor (D) and acceptor (A) are +1.13 V (Quinuclidine/Quinuclidine$^+$; for cyclic voltammetry see ESI, Fig. S6†) and −1.14 V *vs.* Ag/Ag^+ (PMI/PMI^-),[10] respectively, in the reference solvent butyronitrile with a relative permittivity ε_{ref} = 20.7. The zero-zero transition energy E_{00} of the chromophore varies slightly with solvent. The distance (R_{cc}) between the center of the donor (the tertiary amine in the quinuclidine ring) and that of the acceptor (PMI) is 9.85 Å from a molecular model (see ESI Fig. S8†). The effective radii of the donor (r^+) radical cation and acceptor (r^-) radical anion are obtained from the estimated volumes,[48] giving 3.5 Å and 4.3 Å, respectively. The results are shown in Table 2. The free energies for full CS, ΔG_{CS}, in PMI-quinuclidine calculated from eqn (1) are −0.117, −0.116 and −0.057 eV in DMF, MeCN and PrCN, respectively. In Tol, DCM and THF, ΔG_{CS} is positive: 0.958, 0.111 and 0.175 eV, in agreement with the absence of intramolecular charge transfer. The energy level scheme pertaining to the CS dynamics in the PMI-cinchona system in different solvents is illustrated in Fig. 2. The energy level of the CS state in PrCN is close to that of the S_1 state, in principle allowing equilibration, but the ΔG_{CS}, −0.057 eV, is still sufficient to shift the equilibrium mostly to the CS form.[49] As a consequence, the reverse charge transfer from the CS state to the LE state can be ignored.

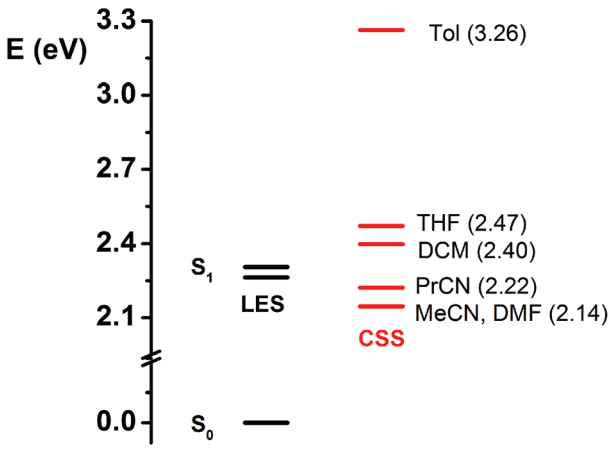

Fig. 2 Energy level scheme for PMI-BnCPD **1** in different solvents calculated with eqn (1) and the parameters given in Table 2 and the E_{00} values for each solvent. LES = locally excited state, CSS = charge separated state. LES levels of **1** in different solvents are in the range 2.26–2.31 eV.

3.1.2 Femtosecond transient absorption (fs-TA) spectroscopy. To further investigate the intramolecular fluorescence quenching process in PMI-BnCPD **1** in different polarity solvents (TOL, DCM, THF, PrCN, MeCN and DMF), femtosecond transient absorption spectroscopy was applied (see Fig. 3). Such experiments were also carried out with PMI-dHQD **2**, but since the results are very similar to those obtained with **1**, they are not reported here.

Table 2 Reduction potentials of quinuclidine (D) and perylene imide (A) in PrCN (in V *vs.* Ag/Ag^+), excitation energy of PMI, and estimation of the driving force (eqn (1)) for charge separation in the excited state using ion radii r and center-to-center distance R_c

E_{ox} D/D^+ (V)	E_{red} A/A^- (V)	E_{00} (eV)	r [D^+] (Å)	r [A^-] (Å)	R_{cc} (Å)	Dielectric constant	ΔG_{CS} (eV)
1.13	−1.14	2.279	3.5	4.3	9.85	20.7	−0.057

 This journal is © The Royal Society of Chemistry and Owner Societies 2019

Published on 13 December 2018. Downloaded by Universiteit van Amsterdam on 4/7/2020 1:17:18 PM.

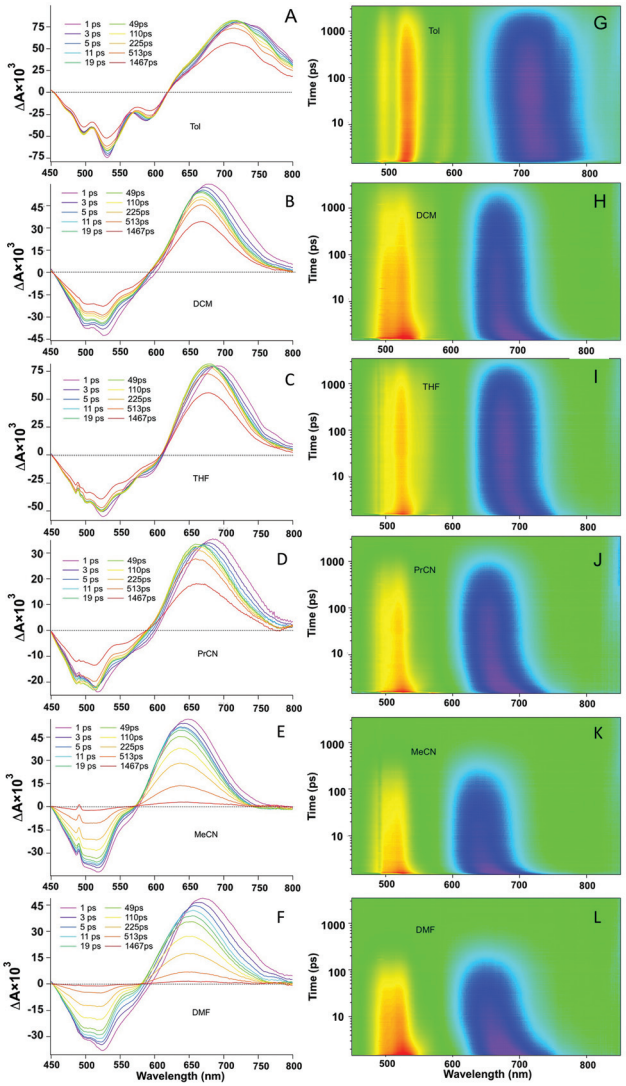

Fig. 3 A–F: fs-TA spectra obtained for compound **1** at the specified time delays in the solvents indicated after photo-excitation at 488 nm at room temperature. G–L: 2D representation of the full data sets. Intensity is represented by colors: $\Delta A < 0$ yellow – red; $\Delta A > 0$ blue – purple.

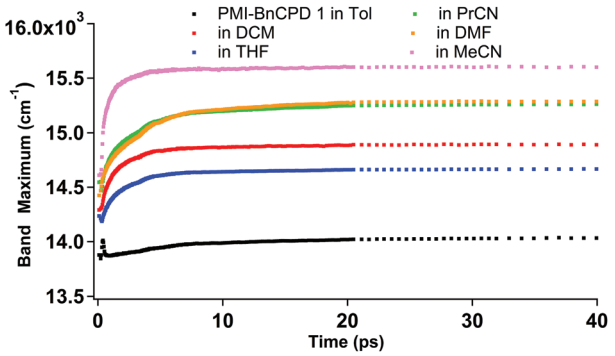

Fig. 4 Shift of the position of the excited state absorption maximum in time of PMI-BnCPD **1** in different solvents.

Considering the steady-state spectral data (Table 1, Fig. 1 and Fig. S2†), the negative peaks at ~500 nm and ~525 nm, can be attributed to ground state depopulation of the PMI chromophore. The negative signals at ~550 nm and ~575 nm come from the stimulated emission of the PMI chromophore. The strong positive absorption bands (between 600 and 800 nm) can be assigned to the S_1 to S_n excited state absorption (ESA) of the perylene monoimide in the locally excited state (LES) or to the charge separated state (CSS) (see below). Overall, the decay rate of the transient spectral features is faster in more polar solvents.

The fast blue shift of the positive absorption band in the first ~10 ps is due to relaxation processes, including vibrational cooling and solvation (Fig. 4).[50–55] By fitting the position of the absorption maximum *vs.* time to a sum of two exponentials, we can characterize the relaxation dynamics of **1** in 6 solvents with the time constants τ_1 and τ_2 with amplitudes a_1 and a_2 (cm^{-1}), and the average relaxation time $\tau_{av} = (\sum a_i\tau_i^2)/(\sum a_i\tau_i)$ (Table 3).[54,56–59]

Fig. 4 and Table 3 show that the peak of the ESA band is shifting more to the blue in more polar solvents, indicating that the S_1 state is more polar (more solvated) than the S_n state (see also Fig. 7). Consistently, the total shift in the first 10 ps increases with increasing solvent polarity. The relaxation is complete within 20 ps after optical excitation, depending on the solvent used. For instance, it is extremely fast in MeCN (0.8 ps, see Table 3) compared to that in toluene. In non-polar solvents, the solvation process has a minor effect on the spectral dynamics of the ESA band. Vibrational cooling effects on the spectra are not expected to depend much on the solvent polarity. Consequently, for compound **1**, in polar solvents the solvation process is the dominant factor in the spectral dynamics of the ESA signal, and the vibrational cooling has a minor contribution.

The fluorescence results clearly point to the occurrence of a quenching process in **1** and **2** in polar solvents, most likely electron transfer, but the transient absorption spectra at first sight give no evidence for this. As reported by Lindsey *et al.*,[11] however, the absorption spectrum of the radical anion of the perylenemonoimide ($PMI^{-\bullet}$) shows an absorption maximum at ~650 nm, very similar to the $S_1 \rightarrow S_n$ absorption. In order to disentangle the spectra of the different electronic states, a more detailed analysis is required.

Table 3 Time constants and amplitudes describing the shift of the excited state absorption maxima and corresponding average relaxation time τ_{av} for PMI-BnCPD **1** in 6 solvents

Solvent	τ_1 (ps)/$a_1 \times 10^{-2}$ (cm^{-1})	τ_2 (ps)/$a_2 \times 10^{-2}$ (cm^{-1})	τ_{av} (ps)	Total shift $\times 10^{-2}$ (cm^{-1})
TOL	5.0/1.3	16/40	7.6	1.6
DCM	0.9/4.3	4.3/1.7	1.9	6.0
THF	1.6/4.1	9.1/0.7	2.7	4.8
PrCN	1.4/4.7	5.5/3.3	3.1	7.9
DMF	2.2/5.4	6.6/3.3	3.9	8.7
MeCN	0.4/7.9	2.5/2.0	0.8	9.9

Published on 13 December 2018. Downloaded by Universiteit van Amsterdam on 4/7/2020 1:17:18 PM.

Global and Target Analysis was performed with Glotaran[60] to obtain a more in-depth view of the photophysical processes.[61] In this way, the time information at all wavelengths of the TA data is analyzed and the kinetic profiles as well as the component spectra are obtained.[62,63]

From the fluorescence experiments we know that there is no intramolecular charge transfer process in compounds **1** and **2** in non-polar solvents. Thus, the global analysis with a sequential model (LES* → LES → GS) is adequate to analyze the TA spectra of compound **1** in the three non-polar solvents. Two decay components are observed, with time constants of 8.4 ps and 3.9 ns in toluene, 2.0 ps and 4.2 ns in DCM, 2.8 ps and 3.9 ns in THF. In agreement with the solvation dynamics study above (Fig. 4 and Table 3), we assign the first lifetime to the fast solvation processes.[54,61,64,65] The LES* species, which corresponds to the black line of EADS in Fig. 5, is converted to the LES (red line in Fig. 5), which has a lifetime of ~4 ns, and decays only the ground state. These longer decay times are in good agreement with TCSPC measurement (Table 1). Because the time window of the TA measurement is rather small, the time constants derived from TCSPC are more accurate. The spectrum of the ESA of the LES of compound **1** in toluene matches the corresponding spectrum of a perylene imide reported by Lindsey *et al.* with a maximum at ~710 nm ($S_1 \rightarrow S_n$ absorption).[10]

For PMI-BnCPD **1** in polar solvents, the additional CS state comes into play. A sequential model (LES* → LES → CSS → GS) is not adequate because the process LES → GS cannot be neglected. Therefore, a target analysis of the excited-state processes was applied.[41,42] The resulting SADS (species associated difference spectra), representing the true spectra of the individual excited species, are shown in Fig. 6. The SADS of the excited state (black line in Fig. 6) shows again the transient absorption features of the PMI* chromophore and fast relaxation processes with time constants of 3.9 ps in PrCN, 3.5 ps in DMF and 0.91 ps in MeCN, respectively, leading to the relaxed singlet LES (red line in Fig. 6), which has a blue-shifted absorption (*e.g.* λ_{max} 690 to 650 nm in DMF). The time constants here are consistent with the solvation dynamics data above (see Table 3). The LES has a lifetime of 1.2 ns in PrCN, 0.20 ns in DMF and 0.31 ns in MeCN, which agree fairly well with the TCSPC results (see Table 1). The SADS reveals the spectral features of the LES of compound **1** in different polar solvents. In the case of polar solvents, the relaxed LE species not only decays to the CS state (with a high rate), but also branches to the ground state relatively slowly, ~4 ns = $(k_f + k_{nr})^{-1}$. The energy level diagram of compound **1** in DMF, with the transitions and the associated time constants is depicted in Fig. 7. The SADS of the last stage (blue line in Fig. 6) shows the spectrum of the CS state (lifetime 2.2 ns in PrCN, 1.9 ns in MeCN and 0.89 ns in DMF), in which the stimulated emission at 575 nm is not observed any longer. This clear spectral evidence further supports the formation of the charge-separated state with the characteristic absorption of the PMI radical anion in polar solvents (PrCN, DMF and MeCN).

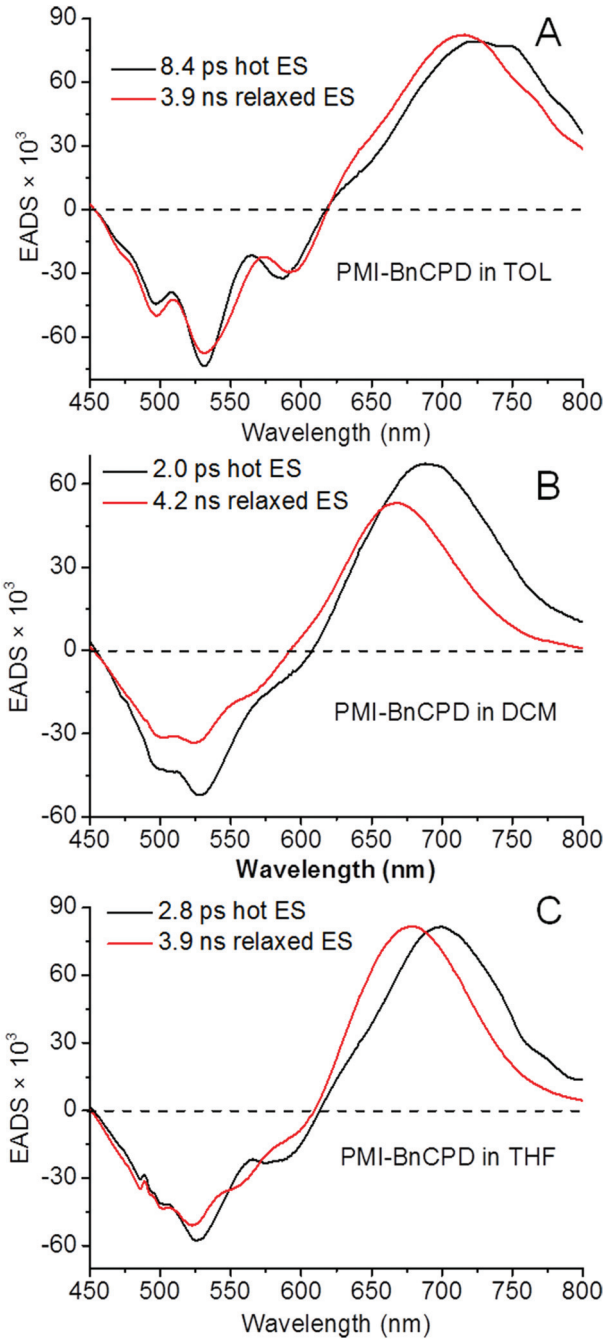

Fig. 5 Compound **1** in Tol (A), DCM (B) and THF (C). Evolution-associated difference spectra (EADS) obtained from the global fitting analysis of femtosecond transient absorption spectra after photoexcitation at 488 nm.The black EADS represents the hot singlet locally excited state LES* while the red one represents the relaxed locally excited state (LES).

To summarize the data on the excited-stated processes of compound **1** in the different polar solvents, the relevant rate constants are collected in Table 4. Because the charge recombination is in the Marcus inverted region, the process becomes faster with the increase of the polarity of the solvent,[66,67] which is consistent with the values in Table 4. We find no evi-

This journal is © The Royal Society of Chemistry and Owner Societies 2019

Published on 13 December 2018. Downloaded by Universiteit van Amsterdam on 4/7/2020 1:17:18 PM.

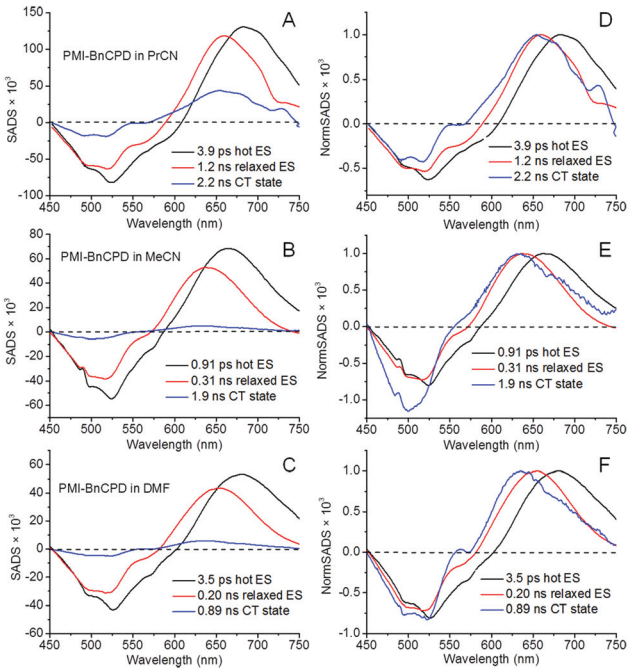

Fig. 6 Compound **1** in PrCN, DMF and MeCN. A–C: Species-associated difference spectra (SADS) resulting from the global target analysis of femtosecond transient absorption spectra after photoexcitation at 488 nm. The black SADS represents the hot locally excited state (LES*), the red SADS represents the relaxed excited state (LES) and the blue SADS belong to the charge separated state (CSS). D–F: normalized SADS.

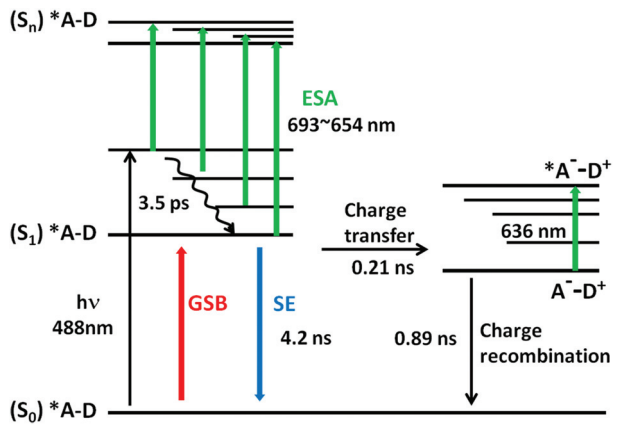

Fig. 7 Energy level diagram of compound **1** in DMF showing the electron-transfer pathway obtained with target analysis, together with the respective decay times corresponding to the states. GSB = ground state bleaching, SE = stimulated emission, ESA = excited state absorption.

dence of the formation of a triplet state, either from the LES or from the CSS.

The fluorescence quantum yields and lifetimes in polar solvents show that the charge separation process is somewhat faster and more efficient in **2** than in **1** in the same solvent. Because the chromophore and the electron donating group are the same in both compounds, the difference is likely to be

Table 4 Rate constants ($\times 10^{-9}$ s^{-1}) for decay of LES to GS (k_0), charge separation (k_{CS}) and charge recombination (k_{CR}) obtained from TCSPC and fsTA experiments on **PMI-BnCPD 1** in polar solvents

Compound	Solvent	τ_f^{-1}	k_0 [a]	k_{CS} [b]	k_{CR}
PMI-BnCPD	PrCN	0.78	0.24	0.54	0.46
	MeCN	2.6	0.23	2.4	0.52
	DMF	4.0	0.24	3.8	1.1

[a] From the fluorescence lifetime $\tau_{f0} = k_0^{-1}$ in polar solvent with TFA, in which the CS process is suppressed. [b] Rate of CS, derived from the fluorescence lifetimes with and without TFA: $k_{cs} = \tau_f^{-1} - \tau_{f0}^{-1}$.

caused by a difference in the electronic coupling, reflecting subtle differences in the molecular geometry. We tried to analyze the structures using DFT and TDDFT calculations, but the number of low-energy conformations for both molecules was so large that meaningful conclusions cannot be reasonably drawn. Details are given in the ESI (Fig. S8†).

3.2 Organocatalytic activity

The parent compound BnCPD is well known as an organocatalyst,[35,68] but the added fluorophore in **1** could in principle interfere with this function. To check the organocatalytic activity of compound **1**, we used a Michael addition reaction with the fluorogenic BODIPY-maleimide **3**, which consists of a BODIPY fluorescent unit and a maleimide as thiol-reactive quenching group.[69] The fluorescence of this probe is very weak (Φ = 0.003) due to the quenching by intramolecular electron transfer to the maleimide. The fluorescence of BODIPY is restored when the maleimide has reacted with the thiol, which

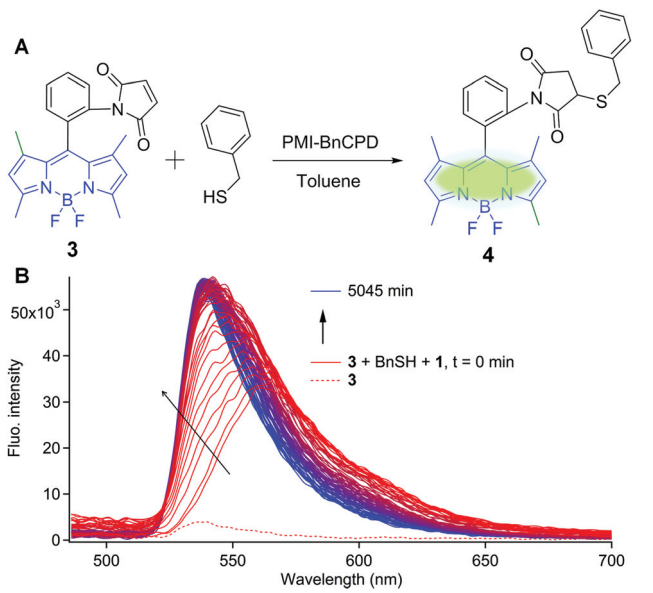

Fig. 8 A: Michael addition of benzyl mercaptan to BODIPY-maleimide **3** catalyzed by **1**. B: Static emission spectra (dashed lines; λ_{exc} = 488 nm) of BODIPY-maleimide **3** (dotted line) and the mixture of BODIPY-maleimide **3**, benzyl mercaptan and **1** as a function of time (solid lines) in toluene leading to strong emission of **4**.

Published on 13 December 2018. Downloaded by Universiteit van Amsterdam on 4/7/2020 1:17:18 PM.

can be used to monitor the organocatalytic activity of compound **1**. As shown in Fig. 8, the fluorescence emission of BODIPY-maleimide (1.1 mM) is very weak ($\lambda_{em,\ max}$ = 528 nm) in toluene. After adding benzyl mercaptan (11.7 mM) and compound **1** (0.1 mM), we can see a strong signal immediately at ~550 nm ($\lambda_{em,\ max}$) attributed to the compound **1**. With the progress of the reaction, the intensity at 528 nm (attributed to the reaction product compound **4**) increased much faster than in the absence of **1**. This demonstrates the organocatalytic activity of compound **1** in the Michael additions of aromatic thiols to maleimide.

4 Conclusions

Upon functionalization with a cinchona organocatalyst the PMI fluorophore becomes very sensitive to its environment. The excited-state lifetimes of **PMI-BnCPD**, **1** and **PMI-dHQD**, **2** are changed from approximately ~4 ns to ~0.2 ns and the quantum yield is decreased from ~0.77 to ~0.03 with the increase of solvent polarity. We show that the fluorescence of the compounds is quenched by charge transfer in polar solvents, in which the tertiary amine of the quinuclidine acts as the electron donor and perylene monoimide acts as the acceptor. The CS species $PMI^{-\bullet}$-$BnCPD^{+\bullet}$ and $PMI^{-\bullet}$-$dHQD^{+\bullet}$ are formed in polar solvents after photoexcitation. Global and target analysis of the femtosecond transient absorption data of PMI-BnCPD **1** were performed and depict spectrally distinguished photoinduced process in different polarity solvents. The locally excited state is formed after rapid relaxation (mostly of the solvent), and characterized by ground state bleaching (450–550 nm), stimulated emission (550–600 nm) and positive absorption features (600–750 nm). In polar solvents, charge separation occurs. The ESA band of the CS state is only slightly blue-shifted relative to that of the LE state. It resembles the published spectrum of the PMI radical anion, and the lack of the stimulated emission feature supports the assignment. The charge separation process can be suppressed when the catalyst binds to H^+, restoring the fluorescence. Both LES and CSS decay to the ground state. We find no evidence of formation of a triplet state. Fluorescently labeled cinchona alkaloid **1** was shown to act as catalyst in a Michael addition. Combined with single molecule techniques, this kind of molecule will have broader application in mechanistic studies in organocatalysis, which will be further elaborated on in our future research.

Conflicts of interest

There are no conflicts of interest to declare.

Acknowledgements

We thank the China Scholarship Council for a scholarship (no. 201406170063) to Dongdong Zheng. Fengshou Yu is gratefully acknowledged for the electrochemistry measurement. Steven Kettelarij performed the synthesis of PMI-dHQD **2**. Michiel Hilbers helped with the spectroscopy experiments.

References

1 T. S. Kaufman and E. A. Rúveda, The quest for quinine: those who won the battles and those who won the war, *Angew. Chem., Int. Ed.*, 2005, **44**, 854–885.
2 M. Li, X.-S. Xue and J.-P. Cheng, Mechanism and Origins of Stereoinduction in Natural Cinchona Alkaloid Catalyzed Asymmetric Electrophilic Trifluoromethylthiolation of β-Keto Esters with N-Trifluoromethylthiophthalimide as Electrophilic SCF_3 Source, *ACS Catal.*, 2017, **7**, 7977–7986.
3 S.-X. Cao, J.-X. Wang and Z.-J. He, Magnetic nanoparticles supported cinchona alkaloids for asymmetric Michael addition reaction of 1, 3-dicarbonyls and maleimides, *Chin. Chem. Lett.*, 2018, **29**, 201–204.
4 M. Rueping, X. Liu, T. Bootwicha, R. Pluta and C. Merkens, Catalytic enantioselective trifluoromethylthiolation of oxindoles using shelf-stable N-(trifluoromethylthio) phthalimide and a cinchona alkaloid catalyst, *Chem. Commun.*, 2014, **50**, 2508–2511.
5 J. D. Duan and P. F. Li, Asymmetric organocatalysis mediated by primary amines derived from cinchona alkaloids: recent advances, *Catal. Sci. Technol.*, 2014, **4**, 311–320.
6 M. N. Grayson and K. Houk, Cinchona Alkaloid-Catalyzed Asymmetric Conjugate Additions: The Bifunctional Brønsted Acid–Hydrogen Bonding Model, *J. Am. Chem. Soc.*, 2016, **138**, 1170–1173.
7 J.-L. Zhu, Y. Zhang, C. Liu, A.-M. Zheng and W. Wang, Insights into the dual activation mechanism involving bifunctional cinchona alkaloid thiourea organocatalysts: An NMR and DFT study, *J. Org. Chem.*, 2012, **77**, 9813–9825.
8 T. Marcelli and H. Hiemstra, Cinchona alkaloids in asymmetric organocatalysis, *Synthesis*, 2010, 1229–1279.
9 J. Guo, Z.-H. Lin, K.-B. Chen, Y. Xie, A. S. Chan, J. Weng and G. Lu, Asymmetric amination of 2-substituted indolin-3-ones catalyzed by natural cinchona alkaloids, *Org. Chem. Front.*, 2017, **4**, 1400–1406.
10 S. I. Yang, R. K. Lammi, S. Prathapan, M. A. Miller, J. Seth, J. R. Diers, D. F. Bocian, J. S. Lindsey and D. Holten, Synthesis and excited-state photodynamics of perylene-porphyrin dyads. Part 3. Effects of perylene, linker, and connectivity on ultrafast energy transfer, *J. Mater. Chem.*, 2001, **11**, 2420–2430.
11 C. Kirmaier, S. I. Yang, S. Prathapan, M. A. Miller, J. R. Diers, D. F. Bocian, J. S. Lindsey and D. Holten, Synthesis and excited-state photodynamics of perylene-porphyrin dyads. 4. Ultrafast charge separation and charge recombination between tightly coupled units in polar media, *Res. Chem. Intermed.*, 2002, **28**, 719–740.

 This journal is © The Royal Society of Chemistry and Owner Societies 2019

Published on 13 December 2018. Downloaded by Universiteit van Amsterdam on 4/7/2020 1:17:18 PM.

12 L. Huang and S.-W. Tam-Chang, N-(2-(N′, N′-Diethylamino) ethyl) perylene-3, 4-dicarboximide and its Quaternized Derivatives as Fluorescence Probes of Acid, Temperature, and Solvent Polarity, *J. Fluoresc.*, 2011, **21**, 213–222.
13 J. S. High, K. A. Virgil and E. Jakubikova, Electronic Structure and Absorption Properties of Strongly Coupled Porphyrin–Perylene Arrays, *J. Phys. Chem. A*, 2015, **119**, 9879–9888.
14 J. Cremer, E. Mena-Osteritz, N. G. Pschierer, K. Müllen and P. Bäuerle, Dye-functionalized head-to-tail coupled oligo (3-hexylthiophenes)—perylene–oligothiophene dyads for photovoltaic applications, *Org. Biomol. Chem.*, 2005, **3**, 985–995.
15 J. Cremer and P. Bäuerle, Perylene–oligothiophene–perylene triads for photovoltaic applications, *Eur. J. Org. Chem.*, 2005, 3715–3723.
16 J. Jacob, S. Sax, T. Piok, E. J. List, A. C. Grimsdale and K. Müllen, Ladder-type pentaphenylenes and their polymers: efficient blue-light emitters and electron-accepting materials via a common intermediate, *J. Am. Chem. Soc.*, 2004, **126**, 6987–6995.
17 T. D. Bell, J. Jacob, M. Angeles-Izquierdo, E. Fron, F. Nolde, J. Hofkens, K. Müllen and F. C. De Schryver, Charge transfer enhanced annihilation leading to deterministic single photon emission in rigid perylene end-capped polyphenylenes, *Chem. Commun.*, 2005, 4973–4975.
18 T. Weil, U. M. Wiesler, A. Herrmann, R. Bauer, J. Hofkens, F. C. De Schryver and K. Müllen, Polyphenylene dendrimers with different fluorescent chromophores asymmetrically distributed at the periphery, *J. Am. Chem. Soc.*, 2001, **123**, 8101–8108.
19 T. Weil, E. Reuther, C. Beer and K. Müllen, Synthesis and characterization of dendritic multichromophores based on rylene dyes for vectorial transduction of excitation energy, *Chem. – Eur. J.*, 2004, **10**, 1398–1414.
20 A. Petrella, J. Cremer, L. De Cola, P. Bäuerle and R. M. Williams, Charge Transfer Processes in Conjugated Triarylamine– Oligothiophene– Perylenemonoimide Dendrimers, *J. Phys. Chem. A*, 2005, **109**, 11687–11695.
21 Q. Wang, S. M. Zakeeruddin, J. Cremer, P. Bäuerle, R. Humphry-Baker and M. Grätzel, Cross surface ambipolar charge percolation in molecular triads on mesoscopic oxide films, *J. Am. Chem. Soc.*, 2005, **127**, 5706–5713.
22 J. Cremer and P. Bäuerle, Star-shaped perylene–oligothiophene–triphenylamine hybrid systems for photovoltaic applications, *J. Mater. Chem.*, 2006, **16**, 874–884.
23 T. D. Bell, A. Stefan, V. Lemaur, S. Bernhardt, K. Müllen, J. Cornil, D. Beljonne, J. Hofkens, M. Van der Auweraer and F. C. De Schryver, Non-conjugated, phenyl assisted coupling in through bond electron transfer in a perylenemonoimide–triphenylamine system, *Photochem. Photobiol. Sci.*, 2007, **6**, 406–415.
24 R. T. Hayes, M. R. Wasielewski and D. Gosztola, Ultrafast photoswitched charge transmission through the bridge molecule in a donor– bridge– acceptor system, *J. Am. Chem. Soc.*, 2000, **122**, 5563–5567.
25 K.-Y. Tomizaki, P. Thamyongkit, R. S. Loewe and J. S. Lindsey, Practical synthesis of perylene-monoimide building blocks that possess features appropriate for use in porphyrin-based light-harvesting arrays, *Tetrahedron*, 2003, **59**, 1191–1207.
26 K.-Y. Tomizaki, R. S. Loewe, C. Kirmaier, J. K. Schwartz, J. L. Retsek, D. F. Bocian, D. Holten and J. S. Lindsey, Synthesis and photophysical properties of light-harvesting arrays comprised of a porphyrin bearing multiple perylene-monoimide accessory pigments, *J. Org. Chem.*, 2002, **67**, 6519–6534.
27 J. Baffreau, L. Ordronneau, S. Leroy-Lhez and P. Hudhomme, Synthesis of perylene-3, 4-mono (dicarboximide)– fullerene C_{60} dyads as new light-harvesting systems, *J. Org. Chem.*, 2008, **73**, 6142–6147.
28 J. A. Elemans, R. van Hameren, R. J. Nolte and A. E. Rowan, Molecular Materials by Self-Assembly of Porphyrins, Phthalocyanines, and Perylenes, *Adv. Mater.*, 2006, **18**, 1251–1266.
29 Q. Al-Galiby, I. Grace, H. Sadeghi and C. J. Lambert, Exploiting the extended π-system of perylene bisimide for label-free single-molecule sensing, *J. Mater. Chem. C*, 2015, **3**, 2101–2106.
30 M. Mitsui, H. Fukui, R. Takahashi, Y. Takakura and T. Mizukami, Single-Molecule Fluorescence Spectroscopy of Perylene Diimide Dyes in a γ-Cyclodextrin Film: Manifestation of Photoinduced H-Atom Transfer via Higher Triplet (n, π*) Excited States, *J. Phys. Chem. A*, 2017, **121**, 1577–1586.
31 H. Hiemstra and H. Wynberg, Addition of aromatic thiols to conjugated cycloalkenones, catalyzed by chiral β-hydroxy amines. A mechanistic study of homogeneous catalytic asymmetric synthesis, *J. Am. Chem. Soc.*, 1981, **103**, 417–430.
32 R. Helder, R. Arends, W. Bolt, H. Hiemstra and H. Wynberg, Alkaloid catalyzed asymmetric synthesis III the addition of mercaptans to 2-cyclohexene-1-one; determination of enantiomeric excess using ^{13}C NMR, *Tetrahedron Lett.*, 1977, **18**, 2181–2182.
33 G. Tanriver, B. Dedeoglu, S. Catak and V. Aviyente, Computational Studies on Cinchona Alkaloid-Catalyzed Asymmetric Organic Reactions, *Acc. Chem. Res.*, 2016, **49**, 1250–1262.
34 T. Marcelli, Organocatalysis: cinchona catalysts, *Wiley Interdiscip. Rev.: Comput. Mol. Sci.*, 2011, **1**, 142–152.
35 T. Kumpulainen, J. Qian and A. M. Brouwer, Spectroscopic Study of a Cinchona Alkaloid-Catalyzed Henry Reaction, *ACS Omega*, 2018, **3**, 1871–1880.
36 W. Qin, A. Vozza and A. M. Brouwer, Photophysical properties of cinchona organocatalysts in organic solvents, *J. Phys. Chem. C*, 2009, **113**, 11790–11795.
37 T. Kumpulainen and A. M. Brouwer, Excited-state proton transfer and ion pair formation in a Cinchona organocatalyst, *Phys. Chem. Chem. Phys.*, 2012, **14**, 13019–13026.

Published on 13 December 2018. Downloaded by Universiteit van Amsterdam on 4/7/2020 1:17:18 PM.

38 J. Qian and A. M. Brouwer, Excited state proton transfer in the Cinchona alkaloid cupreidine, *Phys. Chem. Chem. Phys.*, 2010, **12**, 12562–12569.
39 W. Zhang, M. Caldarola, X. Lu, B. Pradhan and M. Orrit, Single-molecule fluorescence enhancement of a near-infrared dye by gold nanorods using DNA transient binding, *Phys. Chem. Chem. Phys.*, 2018, **20**, 20468–20475.
40 N. I. Georgiev, A. R. Sakr and V. B. Bojinov, Design and synthesis of novel fluorescence sensing perylene diimides based on photoinduced electron transfer, *Dyes Pigm.*, 2011, **91**, 332–339.
41 J. Xie, Y. Chen, W. Yang, D. Xu and K. Zhang, Water soluble 1, 8-naphthalimide fluorescent pH probes and their application to bioimagings, *J. Photochem. Photobiol., A*, 2011, **223**, 111–118.
42 N. I. Georgiev, M. D. Dimitrova, A. M. Asiri, K. A. Alamry and V. B. Bojinov, Synthesis, sensor activity and logic behaviour of a novel bichromophoric system based on rhodamine 6G and 1, 8-naphthalimide, *Dyes Pigm.*, 2015, **115**, 172–180.
43 S. Malkondu, A highly selective and sensitive perylenebisimide-based fluorescent PET sensor for Al^{3+} determination in MeCN, *Tetrahedron*, 2014, **70**, 5580–5584.
44 P. J. Pacheco-Liñán, M. Moral, M. L. Nueda, R. Cruz-Sánchez, J. Fernández-Sainz, A. Garzón-Ruiz, I. Bravo, M. Melguizo, J. Laborda and J. Albaladejo, Study on the pH Dependence of the Photophysical Properties of a Functionalized Perylene Bisimide and Its Potential Applications as a Fluorescence Lifetime Based pH Probe, *J. Phys. Chem. C*, 2017, **121**, 24786–24797.
45 D. Wu, A. C. Sedgwick, T. Gunnlaugsson, E. U. Akkaya, J. Yoon and T. D. James, Fluorescent chemosensors: the past, present and future, *Chem. Soc. Rev.*, 2017, **46**, 7105–7123.
46 B. Daly, J. Ling and A. P. De Silva, Current developments in fluorescent PET (photoinduced electron transfer) sensors and switches, *Chem. Soc. Rev.*, 2015, **44**, 4203–4211.
47 A. Weller, Photoinduced electron transfer in solution: exciplex and radical ion pair formation free enthalpies and their solvent dependence, *Z. Phys. Chem.*, 1982, **133**, 93–98.
48 H. Oevering, M. N. Paddon-Row, M. Heppener, A. M. Oliver, E. Cotsaris, J. W. Verhoeven and N. S. Hush, Long-range photoinduced through-bond electron transfer and radiative recombination via rigid nonconjugated bridges: distance and solvent dependence, *J. Am. Chem. Soc.*, 1987, **109**, 3258–3269.
49 P. Atkins, J. De Paula and J. Keeler, *Atkins' physical chemistry*, Oxford University Press, 2018.
50 C. Reichardt and T. Welton, *Solvents and Solvent Effects in Organic Chemistry*, Wiley-VCH, Weinheim, 2013.
51 Š. Vajda, R. Jimenez, S. J. Rosenthal, V. Fidler, G. R. Fleming and E. W. Castner, Femtosecond to nanosecond solvation dynamics in pure water and inside the γ-cyclodextrin cavity, *J. Chem. Soc., Faraday Trans.*, 1995, **91**, 867–873.
52 R. Jimenez, G. R. Fleming, P. Kumar and M. Maroncelli, dynamics of water, *Nature*, 1994, **369**, 471–473.
53 S. J. Rosenthal, X. Xie, M. Du and G. R. Fleming, Femtosecond solvation dynamics in acetonitrile: Observation of the inertial contribution to the solvent response, *J. Chem. Phys.*, 1991, **95**, 4715–4718.
54 B. Bagchi and B. Jana, Solvation dynamics in dipolar liquids, *Chem. Soc. Rev.*, 2010, **39**, 1936–1954.
55 T. Kumpulainen, B. Lang, A. Rosspeintner and E. Vauthey, Ultrafast Elementary Photochemical Processes of Organic Molecules in Liquid Solution, *Chem. Rev.*, 2016, **117**, 10826–10939.
56 E. W. Castner Jr., M. Maroncelli and G. R. Fleming, Subpicosecond resolution studies of solvation dynamics in polar aprotic and alcohol solvents, *J. Chem. Phys.*, 1987, **86**, 1090–1097.
57 S. J. Rosenthal, R. Jimenez, G. R. Fleming, P. Kumar and M. Maroncelli, Solvation dynamics in methanol: Experimental and molecular dynamics simulation studies, *J. Mol. Liq.*, 1994, **60**, 25–56.
58 T. Fonseca and B. M. Ladanyi, Solvation dynamics in methanol: solute and perturbation dependence, *J. Mol. Liq.*, 1994, **60**, 1–24.
59 D. Bingemann and N. P. Ernsting, Femtosecond solvation dynamics determining the band shape of stimulated emission from a polar styryl dye, *J. Chem. Phys.*, 1995, **102**, 2691–2700.
60 J. J. Snellenburg, S. P. Laptenok, R. Seger, K. M. Mullen and I. H. M. van Stokkum, Glotaran: a Java-based graphical user interface for the R package TIMP, *J. Stat. Softw.*, 2012, **49**, 1–22.
61 C. Hippius, I. H. M. van Stokkum, E. Zangrando, R. M. Williams and F. Würthner, Excited state interactions in calix [4] arene-perylene bisimide dye conjugates: Global and target analysis of supramolecular building blocks, *J. Phys. Chem. C*, 2007, **111**, 13988–13996.
62 R. Berera, R. van Grondelle and J. T. Kennis, Ultrafast transient absorption spectroscopy: principles and application to photosynthetic systems, *Photosynth. Res.*, 2009, **101**, 105–118.
63 J. Ravensbergen, F. F. Abdi, J. H. van Santen, R. N. Frese, B. Dam, R. van de Krol and J. T. Kennis, Unraveling the carrier dynamics of $BiVO_4$: A femtosecond to microsecond transient absorption study, *J. Phys. Chem. C*, 2014, **118**, 27793–27800.
64 G. Schweitzer, R. Gronheid, S. Jordens, M. Lor, G. De Belder, T. Weil, E. Reuther, K. Müllen and F. C. De Schryver, Intramolecular directional energy transfer processes in dendrimers containing perylene and terrylene chromophores, *J. Phys. Chem. A*, 2003, **107**, 3199–3207.
65 G. De Belder, S. Jordens, M. Lor, G. Schweitzer, R. De, T. Weil, A. Herrmann, U. K. Wiesler, K. Müllen and F. C. De Schryver, Femtosecond fluorescence upconversion study of rigid dendrimers containing peryleneimide chromophores at the rim, *J. Photochem. Photobiol., A*, 2001, **145**, 61–70.

 This journal is © The Royal Society of Chemistry and Owner Societies 2019

Published on 13 December 2018. Downloaded by Universiteit van Amsterdam on 4/7/2020 1:17:18 PM.

66 N. Mataga, H. Chosrowjan, S. Taniguchi, Y. Shibata, N. Yoshida, A. Osuka, T. Kikuzawa and T. Okada, Ultrafast Charge Separation from the S_2 Excited State of Directly Linked Porphyrin– Imide Dyads: First Unequivocal Observation of the Whole Bell-Shaped Energy-Gap Law and Its Solvent Dependencies, *J. Phys. Chem. A*, 2002, **106**, 12191–12201.

67 E. H. A. Beckers, S. C. J. Meskers, A. P. H. J. Schenning, Z. Chen, F. Würthner and R. A. J. Janssen, Charge separation and recombination in photoexcited oligo (p-phenylene vinylene): Perylene bisimide arrays close to the marcus inverted region, *J. Phys. Chem. A*, 2004, **108**, 6933–6937.

68 J. Kaur, N. Islam, A. Kumar, V. K. Bhardwaj and S. S. Chimni, Organocatalytic enantioselective synthesis of C_3 functionalized indole derivatives, *Tetrahedron*, 2016, **72**, 8042–8049.

69 T. Matsumoto, Y. Urano, T. Shoda, H. Kojima and T. Nagano, A thiol-reactive fluorescence probe based on donor-excited photoinduced electron transfer: key role of ortho substitution, *Org. Lett.*, 2007, **9**, 3375–3377.